Journal of Hydrology xxx (2015) xxx–xxx

Contents lists available at ScienceDirect

Journal of Hydrology

journal homepage: www.elsevier.com/locate/jhydrol

Rainwater catchment system design using simulated future climate data

Corey D. Wallace *, Ryan T. Bailey, Mazdak Arabi

Department of Civil and Environmental Engineering, Colorado State University, 1372 Campus Delivery, Fort Collins, CO 80523-1372, United States

ARTICLE INFO

Article history:
Received 22 May 2015
Received in revised form 31 July 2015
Accepted 8 August 2015
Available online xxxx
This manuscript was handled by Konstantine P. Georgakakos, Editor-in-Chief, with the assistance of Michael Bruen, Associate Editor

Keywords:
Rainwater supply
Rain catchment systems
General circulation models

SUMMARY

Rainwater harvesting techniques are used worldwide to augment potable water supply, provide water for small-scale irrigation practices, increase rainwater-use efficiency for sustained crop growth in arid and semi-arid regions, decrease urban stormwater flow volumes, and in general to relieve dependency on urban water resources cycles. A number of methods have been established in recent years to estimate reliability of rainwater catchment systems (RWCS) and thereby properly size the components (roof catchment area, storage tank size) of the system for a given climatic region. These methods typically use historical or stochastically-generated rainfall patterns to quantify system performance and optimally size the system, with the latter accounting for possible rainfall scenarios based on statistical relationships of historical rainfall patterns. To design RWCS systems that can sustainably meet water demand under future climate conditions, this paper introduces a method that employs climatic data from general circulation models (GCMs) to develop a suite of catchment area vs. storage size design curves that capture uncertainty in future climate scenarios. Monthly rainfall data for the 2010–2050 time period is statistically downscaled to daily values using a Markov chain algorithm, with results used only from GCMs that yield rainfall patterns that are statistically consistent with historical rainfall patterns. The process is demonstrated through application to two climatic regions of the Federated States of Micronesia (FSM) in the western Pacific, wherein the majority of the population relies on rainwater harvesting for potable water supply. Through the use of design curves, communities can provide household RWCS that achieve a certain degree of storage reliability. The method described herein can be applied generally to any geographic region. It can be used to first, assess the future performance of existing household systems; and second, to design or modify systems that will yield adequate storage for future climate conditions.

1. Introduction

Rainwater harvesting techniques are used worldwide to augment potable water supply (Sturm et al., 2009; Zhang et al., 2009; Jones and Hunt, 2010; Rowe, 2011; Opare, 2012), provide water for small-scale irrigation practices (Helmreich and Horn, 2008), sustain crop growth in arid and semi-arid regions by improving rainwater-use efficiency (Oweis and Hachum, 2006; Biazin et al., 2012), manage stormwater and decrease risk of flooding through decreasing urban stormwater flow volumes (Chilton et al., 1999; Basinger et al., 2010; Steffen et al., 2013), facilitate green building applications (Guo and Baetz, 2007), and in general relieve dependency on urban water resources cycles (Diagger, 2009; Basinger et al., 2010). Rainwater catchment systems (RWCS) often consist of an impermeable-surface rooftop, a storage tank, and a conveyance system between the rooftop and the tank. Due to drought concerns, several countries (e.g. Bermuda, Jordan) have mandated installation of RWCS for new homes and buildings (Abdulla and Al-Shareef, 2009; Rowe, 2011), with several regions increasing implementation due to restrictions on use of public water supply (Jones and Hunt, 2010; Li et al., 2010). Recent studies have estimated that a significant portion (25–60%) of urban household potable water demand could be reduced by using harvested rainwater (Coombes et al., 1999; Dixon et al., 1999; Herrmann and Schmida, 1999; CIRIA, 2001; Ghisi, 2006; Ghisi et al., 2007; Abdulla and Al-Shareef, 2009; Zhang et al., 2009).

Roof catchment area size and storage tank capacity typically are the targeted system parameters for system design. A number of RWCS design techniques have been developed, each with the general objective of providing guidelines for catchment area/storage tank capacity combinations that will yield a certain level of reliability, with system reliability defined as the portion of time that the system will meet water demand. For a comprehensive review of RWCS sizing methods, the reader is referred to Basinger et al. (2010). Design curves often are used, with each curve representing the ensemble of catchment area/tank size combinations that will

* Corresponding author. Tel.: +1 970 491 5045; fax: +1 970 491 7727.
E-mail addresses: cdwallac@gmail.com (C.D. Wallace), rtbailey@engr.colostate.edu (R.T. Bailey), mazdak.arabi@colostate.edu (M. Arabi).

http://dx.doi.org/10.1016/j.jhydrol.2015.08.006
0022-1694/

provide a certain level of reliability (e.g. 90%). At the most basic level, approaches consider only fluctuation in annual historical precipitation depth to develop design curves (Fewkes, 1999; Gould and Nissen-Petersen, 1999; Ngigi, 1999). A more accurate approach is to use series of long-term historical daily rainfall depths, with daily depths and daily water demand input into a water balance algorithm (Jenkins et al., 1978) to determine end-of-day stored volume and spilled water for various combinations of catchment area and tank size (Herrmann and Schmida, 1999; Liaw and Tsai, 2004; Roebuck and Ashley, 2006; Su et al., 2009; Han and Ki, 2010; Khastagir and Jayasuriya, 2010; Ward et al., 2010; Palla et al., 2011; Mun and Han, 2012; Liaw and Chiang 2014).

With the realization that systems designed using historical rainfall patterns may not be accurately sized for the range of possible future rainfall patterns, several recent studies have used stochastically-generated series of rainfall to assess system performance and create design curves. Parametric approaches (e.g. Guo and Baetz, 2007) use statistical parameters to represent precipitation series, whereas non-parametric approaches (Cowden et al., 2008; Basinger et al., 2010) generate ensembles of synthetic time series using a Markov chain algorithm (Lall et al., 1996; Sharma and Lall, 1999), i.e. probabilities of precipitation occurrence and daily event sequence (i.e. wet day following a wet day, dry day following a wet day, etc.) and are more resilient to the presence of outliers (Lanzante, 1996). An alternative to using stochastic precipitation generators as a means to provide possible rainfall pattern scenarios is to use rainfall data from future climate projections, as output by general circulation models (GCMs). To our knowledge, no studies have utilized GCM output data in creating RWCS design guidelines.

The objective of this study is to demonstrate the use of projected climate data from GCMs to assist in developing RWCS design curves for varying levels of reliability. Future rainfall data, derived from GCM output, and water demand rates are input to a RWCS daily water balance algorithm, with an algorithm used to identify required roof catchment areas and storage tank capacities to yield adequate water supply in the future at various levels of reliability. Sub-objectives pertaining to climate data include statistical downscaling of monthly rainfall values to daily values using a Markov chain algorithm, followed by the use of a multi-criteria score-based method (Fu et al., 2013) to select the best-performing GCMs for the given study region using probability density function (PDF) analysis (Perkins et al., 2007). An ensemble of curves for each reliability level is obtained, thereby incorporating uncertainty into the design process for RWCS. The methodology is applied to two climate regions of the Federated States of Micronesia (FSM), an insular nation of islands covering more than 2 million km^2 of the western Pacific Ocean, and where household rainwater harvesting provides the majority of water demand.

2. Methods

This section describes the methodology to use projected rainfall data from GCMs to develop catchment area/storage tank capacity reliability curves for household rooftop RWCS. Following an overview of the RWCS water balance algorithm and its use to provide relationships between catchment area and tank capacity for varying levels of reliability, the downscaling and testing of GCM output data against historical data is presented. The overall process is depicted in Fig. 1. Finally, an application of the methodology to the western and eastern climate regions of the FSM is presented.

2.1. RWCS water balance algorithm

A standard household rooftop RWCS (Fig. 2a) consists of a guttered catchment area, a conveyance system to deliver capture rainwater from the catchment area, and a storage tank. Time-dependent fluctuation of rainwater volume in the tank can be estimated using the water balance algorithm developed by Jenkins et al. (1978). The method accounts for depth of rainfall, water demand, guttered roof catchment area, storage tank capacity, and gutter system conveyance efficiency. The latter is defined as the portion of rainwater volume that is delivered from the catchment area to the storage tank after losses due to leakage or spillage. The volume stored at the end of the selected time step is calculated as:

$$V_t = \max\{V_{t-1} + \min[(AP_t\varepsilon), (S - V_{t-1})] - O_t, 0\} \quad (1)$$

where V_t is the volume of stored rainwater (L^3) at the end of the current time t, V_{t-1} is the stored rainwater volume (L^3) at the previous time step, A is the rooftop catchment area (L^2) connected to the guttering system, P_t is the depth of precipitation (L) for the current time step, ε is the conveyance efficiency, S is the storage tank capacity (L^3), and O_t is the water removed from the tank during the current time step. The algorithm is defined in units of length, L, to illustrate its general application. The volume of captured rainwater volume is calculated by AP_t, which is multiplied by ε to provide the potential volume of water entering the tank. The actual volume entering the tank is constrained by the un-filled storage volume of the current time step ($S - V_{t-1}$). Eq. (1) also handles the case of complete depletion of stored rainwater. Eq. (1) represents the Yield-After-Spillage (YAS) algorithm (Jenkins et al., 1978), in which the water demand O_t is removed from the system after any excess water is allowed to spill via overflow (Fewkes, 1999; Fewkes and Butler, 2000; Mitchell, 2007; Basinger et al., 2010; Mun and Han, 2012). Eq. (1) often is employed using daily time steps to capture small-scale temporal dynamics of rainfall patterns (Fewkes, 1999).

Eq. (1) can be used to develop combinations of roof area and tank size that meet a certain level of reliability, with reliability defined as the portion of time (e.g. 80%, 90%) that the system will meet water demand based on rainfall patterns for a given geographic location. For example, for a given series of daily rainfall data P_t and daily demand O_t, a roof catchment area A is selected, with the tank size S adjusted until the daily end-of-day volumes V_t meet the desired level of reliability. This is repeated for a range of catchment areas until an ensemble of catchment area/tank size combinations is produced (Fig. 2b), with the ensemble (i.e. design curve) used to design new RWCS that will meet a given level of reliability (Fig. 1). Of course, designing for higher reliability rates requires larger catchment areas and/or larger storage tank capacity (Fig. 2b). Historical daily rainfall depths or stochastically-generated daily rainfall depths have been used in this process. Section 2.2 describes the use of projected rainfall data from GCMs to provide the series of daily rainfall to use in the algorithm.

2.2. Daily rainfall series from projected climate

To use daily rainfall rates and patterns from future climate scenarios in the RWCS design curve construction, monthly rainfall output from GCMs participating in the Coupled Model Intercomparison Project 5 (CMIP5) (Meehl et al., 2009; Taylor et al., 2012) is statistically downscaled to daily values, with the downscaled GCM data tested against historical rainfall to identify the best-performing GCMs for a given study region (Fig. 1). The downscaled daily data is used in the GCM assessment due to the tendency of GCMs to overestimate the frequency and underestimate the intensity of daily precipitation depths, often failing to accurately reproduce the statistics seen in historical records (Mearns et al., 1995; Walsh and McGregor, 1995, 1997; Bates et al., 1998; Charles and Bates, 1999). For RWCS analysis and design, capturing the daily dynamics of rainfall patterns is essential, as several days without rainfall can deplete storage tanks.

Please cite this article in press as: Wallace, C.D., et al. Rainwater catchment system design using simulated future climate data. J. Hydrol. (2015), http://dx.doi.org/10.1016/j.jhydrol.2015.08.006

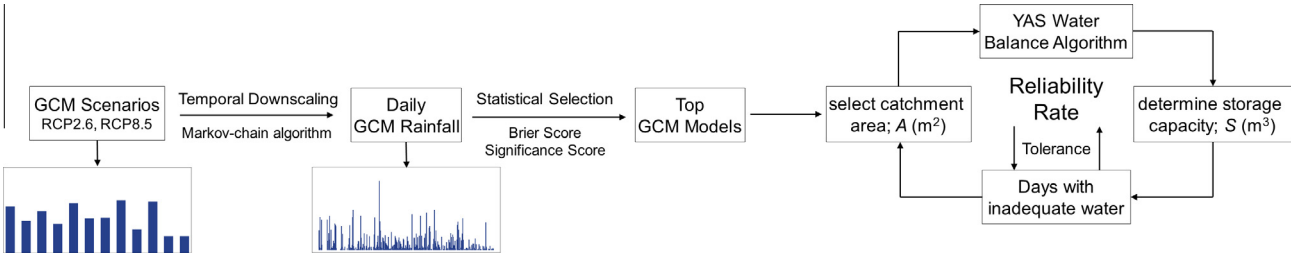

Fig. 1. Representation of the methodology to use projected rainfall data from GCMS to develop catchment area/storage tank capacity reliability curves for household rooftop RWCS. Following temporal downscaling and statistical selection of top GCM datasets, the RWCS water balance algorithm is used to determine system dimensions as their performance converges on a desired reliability rate.

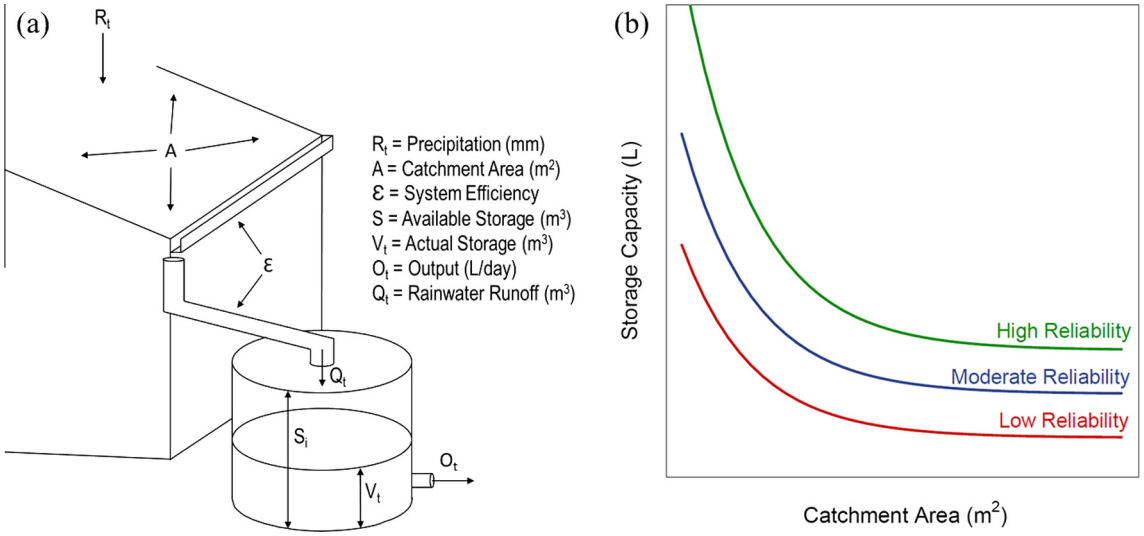

Fig. 2. (a) schematic of a typical RWCS showing the various components, including the storage tank, water transmission system, and rooftop catchment area; (b) general shape of design curves, indicating low, moderate, and high levels of reliability.

2.2.1. Temporal downscaling of future climate data

A Markov chain algorithm is used to downscale monthly GCM rainfall data to daily values using historical rainfall data from the geographic region of interest. Following generation of daily wet/dry and warm/cool sequences for each month of historical data, maximum-likelihood estimation is used to fit shape parameters for a series of monthly gamma distributions for the various classifications, which are then used to compute the precipitation depth for future wet days. Finally, the calculated daily precipitation values are scaled such that the sum of values for each month equals the monthly values from the GCM data.

Good statistical representation of wet/dry, warm/cool probability is essential to an accurate representation of climate patterns. A Markov chain algorithm is a bivariate stochastic process that utilizes transitional probabilities. The algorithm is expressed by:

$$X_t|X_{t-1} \sim \text{Markov}(\boldsymbol{P}, p_1) \quad (2)$$

where $\boldsymbol{P}$ is the transitional probability matrix whose elements p_{ij} are defined by:

$$p_{ij} = \Pr(X_t = i|X_{t-1} = j) \quad i,j = \text{wet or dry} \quad (3)$$

and p_1 is the probability distribution vector of the wet/dry and warm/cool classifications (Srikanthan and McMahon, 2001).

Using historical data, one of two values is assigned to each month: 0 if the month is dry and 1 if the month is wet. To determine the classification of each month, the precipitation depth of that month is compared to a predetermined threshold value, typically the calculated median of average precipitation of each month across all years of data. If the average precipitation of a given month is greater than the median value, it is classified as wet. Conversely, if the average precipitation of that month is less than the median, it is classified as dry. This classification method is performed for the n-month period under consideration, typically as far back as historical data is available, and transitional probability matrices are constructed for application to future periods. A monthly warm/cool classification corresponding to temperature is determined in the same manner.

Using the same methodology, each month in the future dataset is assigned a wet/dry and a warm/cool classification. Once the class of each future month has established, a random historical month of the same class is selected, and the precipitation and temperature values of each day of the historical month are extracted. The wet/dry and warm/cool conditions of each day are determined using the classification methodology previously described; these classifications are then applied to the corresponding days of the future month.

The amount of precipitation that can statistically occur on each day (n) depends on the classifications of the previous day ($n-1$). The statistical model for days with non-zero precipitation is most commonly a gamma distribution (Coe and Stern, 1982; Srikanthan, 2005). For this reason, different precipitation gamma distributions are referenced depending on the wet/dry and warm/cool classifications of each day, making it a first-order process that relies solely on the classifications of the previous day. Using maximum-likelihood estimation, fitted gamma distributions are created for each month of the year, which then are used to

calculate future daily values of precipitation and temperature. More detailed explanation of the Markov chain process can be found in Todorovic and Woolhiser (1975) and Srikanthan and McMahon (2001).

After the Markov model is fitted to historical data, monthly precipitation averages generated by each GCM are used to assign precipitation depth to each day, with daily values retaining the climate patterns forecasted. Each month within the GCM datasets is temporally downscaled using both the wet/dry classification (e.g. 0, 1) and the time-dependent probability of rain (p_{ij}) of each nth day.

2.2.2. Identifying top-performing GCMs

A multi-score method similar to that outlined by Fu et al. (2013) is used to assess the performance of the various downscaled CMIP5 GCMs in comparison with historical daily rainfall data for the geographic region of interest. Effectively, this method determines which GCMs to accept and which ones to reject in the construction of the RWCS design curves. The two scores used in the assessment are the Skill Score (S_{score}) (Perkins et al., 2007) and the Brier Score (BS) (Brier, 1950), both which compare the PDFs of GCM-simulated climate variables to PDFs of historical values. Comparing PDFs rather than evaluation of means (e.g. annual, seasonal, and monthly) or standard deviation provides a more stringent test for climate models, as it quantifies the ability of the models to simulate precipitation on daily time scales (Perkins et al., 2007). This is particularly essential for the design of RWCS, which are strongly sensitive to sub-monthly periods of low rainfall.

The S_{score}, a metric introduced by Perkins et al. (2007) to assess GCM performance for regions in Australia, is used to evaluate the degree to which GCM output captures the attributes of historical climate patterns by measuring the common area between the two PDFs. S_{score} analysis calculates the cumulative minimum value of each binned value for two distributions, quantifying the overlap between the two PDF distributions. Significant overlap (high S_{score} value) between the modeled distribution and the observed data indicates a better replication of historical climate patterns. The score is calculated as:

$$S_{score} = \sum_{i=1}^{n} \mathrm{Min}(P_{mi}, P_{oi}) \tag{4}$$

where P_{mi} is the modeled ith probability value of each bin, P_{oi} is the observed ith probability value of each bin, and n is the number of bins. Perkins et al. (2007) suggest that GCMs with an S_{score} greater than 0.80 provide the best representation of climate.

The BS calculates the measurement of the mean squared difference between the predicted probability of an outcome and the actual outcome, with a minimum value of zero for perfect forecasting and maximum value of 2 for the poorest replication. The score is computed as:

$$BS = \frac{1}{n} \sum_{i=1}^{n} (P_{mi} - P_{oi})^2 \tag{5}$$

where P_{mi} is the modeled ith probability value of each bin, P_{oi} is the observed ith probability value of each bin, and n is the number of bins. Typically the number of bins is fixed at 100. The size of the dataset has an effect on the quality of the Brier Score analysis, with larger sets generally producing a more accurate BS value (Brier, 1950). The S_{score} is used as the primary criteria for assessing GCM output, with the BS score used as a secondary check.

2.3. Application of methodology to the FSM region

2.3.1. Climate and water resources of the FSM

The FSM (Fig. 3) is a geographically isolated nation consisting of 4 larger volcanic islands (Yap, Chuuk, Pohnpei, Kosrae) and 32

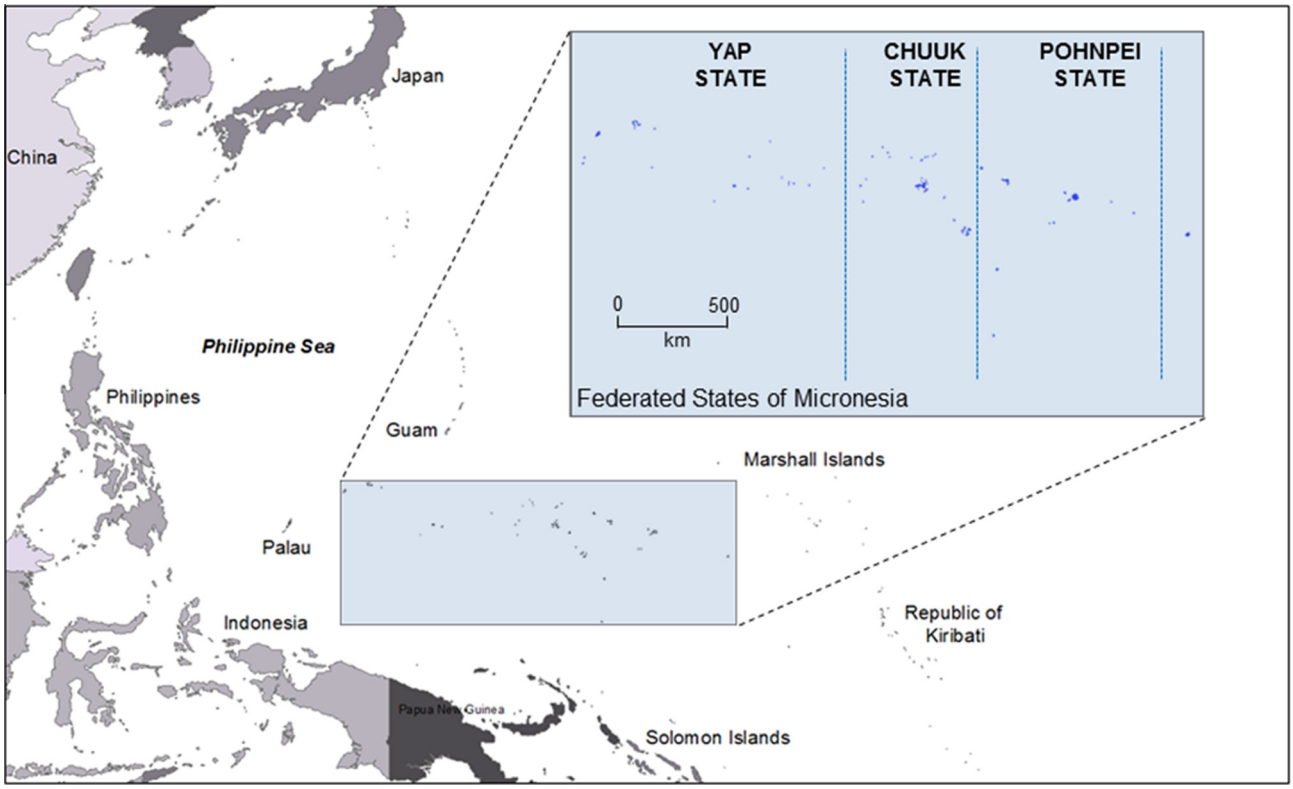

Fig. 3. Map of the western Pacific Ocean showing the location of the Federated States of Micronesia. The eastern (Pohnpei) and western (Yap) regions of the FSM are examined in this study, with regional variation in precipitation depth recognized as a governing parameter in adequate system design.

Please cite this article in press as: Wallace, C.D., et al. Rainwater catchment system design using simulated future climate data. J. Hydrol. (2015), http://dx.doi.org/10.1016/j.jhydrol.2015.08.006

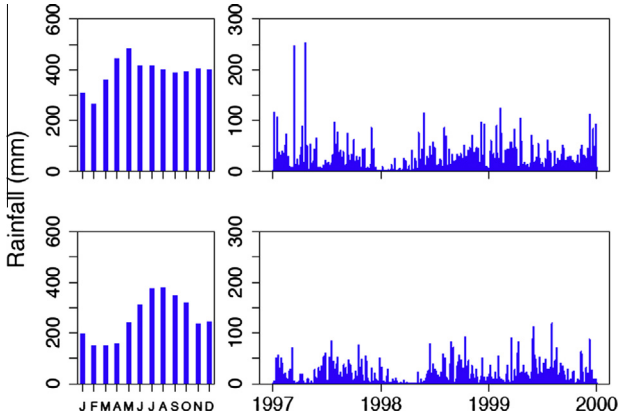

Fig. 4. (left) Average monthly precipitation trend for the eastern (top) and western (bottom) FSM using climate data for the period from 1952 to 2012. (right) Time-series of daily precipitation depths from 1997 to 1999; a major drought occurred in early 1998, placing heavy stress on Micronesian RWCS.

smaller atolls. The nation spans an area of more than 2 million km^2 in the western Pacific Ocean, though total land area amounts to just over 700 km^2. Each atoll consists of a ring-shaped reef structure which entirely or partially encloses a shallow lagoon, with small communities residing on many of the atoll islets. Total population of the FSM is approximately 110,000, with the majority living on the larger volcanic islands and about 4500 residing on the atolls (Micronesia, 2002). The average population of communities living on atolls is about 400.

Annual rainfall depth across the FSM ranges from 3000 to 5200 mm per year, with precipitation depth increasing from west (Yap State) to east (Pohnpei State) due to the western FSM region experiencing a more prolonged dry season (Lander and Khosrowpanah, 2004). Throughout the FSM, the majority of rainfall occurs during the rainy season between April and December, with nearly 50% of the total annual rainfall seen between July and October. The dry season typically extends between December and April, during which time water shortages may occur (Fig. 4). Average temperatures are constant at about 26–27 °C, with a relative

Table 1
CMIP5 climate modeling centers and the names of their corresponding general circulation models.

Modeling center (or group)	ID	Institute ID	Model name
Commonwealth Scientific and Industrial Research Organization (CSIRO) and Bureau of Meteorology (BOM), Australia	1	CSIRO-BOM	ACCESS1.0
	2		ACCESS1.3
Beijing Climate Center, China Meteorological Administration	3	BCC	BCC-CSM1.1
	4		BCC-CSM1.1(m)
Instituto Nacional de Pesquisas Espaciais (National Institute for Space Research)	5	INPE	BESM OA 2.3
College of Global Change and Earth System Science, Beijing Normal University	6	GCESS	BNU-ESM
Canadian Centre for Climate Modelling and Analysis	7	CCCMA	CanESM2
	8		CanCM4
	9		CanAM4
University of Miami – RSMAS	10	RSMAS	CCSM4(RSMAS)*
National Center for Atmospheric Research	11	NCAR	CCSM4
Community Earth System Model Contributors	12	NSF-DOE-NCAR	CESM1(BGC)
	13		CESM1(CAM5)
	14		CESM1(CAM5.1, FV2)
	15		CESM1(FASTCHEM)
	16		CESM1(WACCM)
Center for Ocean-Land-Atmosphere Studies and National Centers for Environmental Prediction	17	COLA and NCEP	CFSv2-2011
Centro Euro-Mediterraneo per I Cambiamenti Climatici	18	CMCC	CMCC-CESM
	19		CMCC-CM
	20		CMCC-CMS
Centre National de Recherches Météorologiques/Centre Européen de Recherche et Formation Avancée en Calcul Scientifique	21	CNRM-CERFACS	CNRM-CM5
	22		CNRM-CM5-2
Commonwealth Scientific and Industrial Research Organization in collaboration with Queensland Climate Change Centre of Excellence	23	CSIRO-QCCCE	CSIRO-Mk3.6.0
EC-EARTH consortium	24	EC-EARTH	EC-EARTH
LASG, Institute of Atmospheric Physics, Chinese Academy of Sciences and CESS, Tsinghua University	25	LASG-CESS	FGOALS-g2
LASG, Institute of Atmospheric Physics, Chinese Academy of Sciences	26	LASG-IAP	FGOALS-gl
	27		FGOALS-s2
The First Institute of Oceanography, SOA, China	28	FIO	FIO-ESM
NASA Global Modeling and Assimilation Office	29	NASA GMAO	GEOS-5
NOAA Geophysical Fluid Dynamics Laboratory	30	NOAA GFDL	GFDL-CM2.1
	31		GFDL-CM3
	32		GFDL-ESM2G
	33		GFDL-ESM2M
	34		GFDL-HIRAM-C180
	35		GFDL-HIRAM-C360
NASA Goddard Institute for Space Studies	36	NASA GISS	GISS-E2-H
	37		GISS-E2-H-CC
	38		GISS-E2-R
	39		GISS-E2-R-CC

(*continued on next page*)

Table 1 (*continued*)

Modeling center (or group)	ID	Institute ID	Model name
National Institute of Meteorological Research/Korea Meteorological Administration	40	NIMR/KMA	HadGEM2-AO
Met Office Hadley Centre (additional HadGEM2-ES realizations contributed by Instituto Nacional de Pesquisas Espaciais)	41	MOHC (additional realizations by INPE)	HadCM3
	42		HadGEM2-CC
	43		HadGEM2-ES
	44		HadGEM2-A
Institute for Numerical Mathematics	45	INM	INM-CM4
Institut Pierre-Simon Laplace	46	IPSL	IPSL-CM5A-LR
	47		IPSL-CM5A-MR
	48		IPSL-CM5B-LR
Japan Agency for Marine-Earth Science and Technology, Atmosphere and Ocean Research Institute (The University of Tokyo), and National Institute for Environmental Studies	49	MIROC	MIROC-ESM
	50		MIROC-ESM-CHEM
Atmosphere and Ocean Research Institute (The University of Tokyo), National Institute for Environmental Studies, and Japan Agency for Marine-Earth Science and Technology	51	MIROC	MIROC4h
	52		MIROC5
Max-Planck-Institut für Meteorologie (Max Planck Institute for Meteorology)	53	MPI-M	MPI-ESM-MR
	54		MPI-ESM-LR
	55		MPI-ESM-P
Meteorological Research Institute	56	MRI	MRI-AGCM3.2H
	57		MRI-AGCM3.2S
	58		MRI-CGCM3
	59		MRI-ESM1
Nonhydrostatic Icosahedral Atmospheric Model Group	60	NICAM	NICAM.09
Norwegian Climate Centre	61	NCC	NorESM1-M
	62		NorESM1-ME

humidity over 80%. Periodic droughts occur, triggered by El Niño Southern Oscillation events which alter ocean temperatures. Intense events can lead to extreme drought conditions, for example during the first few months of 1998 when monthly rainfall depths are the lowest on record during the 1953–2001 period (Fig. 4) (Lander and Khosrowpanah, 2004).

Freshwater supply for island communities on the four high volcanic islands consist of surface water, captured rainwater, and groundwater, whereas communities on the atoll islands rely solely on rainwater captured by RWCS and fresh groundwater (MacCracken et al., 2007; White et al., 2007) due to the lack of surface water bodies. Residents typically rely on rainwater for all domestic purposes (Dillaha and Zolan, 1985; Taboroši and Martin, 2011), with groundwater used only in time of drought. Water quality is typically high (Dillaha and Zolan, 1985) due to the frequency of significant rainfall events and the associated flushing of plant debris and animal feces from the rooftop and gutter systems. During the 1998 drought, the depleted RWCS volumes and depleted fresh groundwater (Bailey et al., 2013) required water importation by boat from the high volcanic islands (Taboroši and Collazo, 2011; Taboroši and Martin, 2011).

2.3.2. RWCS design curve construction

RWCS design curves for various levels of reliability were constructed for the FSM region using the methodology outlined in Sections 2.1 and 2.2. Curves are constructed for the western and eastern FSM regions, since rainfall patterns and depths vary considerably between these two regions. The suite of 62 GCMs assessed is listed in Table 1. We acknowledge the World Climate Research Programme's Working Group on Coupled Modeling, which is responsible for CMIP, and we thank the modeling groups (Table 1) for producing and making available their model output.

Two Representative Concentration Pathways (RCPs 2.6 and 8.5) are used to represent two divergent rates of increase in atmospheric radiative forcing and hence effectively bracket the range of possible future climate scenarios. Extreme climate change mitigation, characterized by drastic policy and lifestyle change, is represented by the RCP2.6 forcing scenario, wherein escalation of radiative forcing is limited to 2.6 W/m^2 at year 2100. Conversely,

Table 2
Results of the multi-score statistical analysis performed on GCMs for the RCP2.6 forcing scenario for the eastern FSM. The Brier Score (*BS*) and significance score (S_{score}) are shown for each of the GCMs analyzed over the 2010–2050 study period. A line indicating the models with $S_{score} > 0.8$ is included to indicate models used in design curve development.

Model	*BS*	S_{score}
CNRM-CM5	0.0023	0.837
GISS-E2-R	0.0024	0.834
GFDL-CM3	0.0025	0.833
FGOALS_g2	0.0027	0.833
BNU-ESM	0.0021	0.830
NorESM1-M	0.0026	0.826
NorESM1-ME	0.0027	0.825
GISS-E2-H	0.0026	0.823
FIO-ESM	0.0033	0.822
MRI-CGCM3	0.0024	0.816
MPI-ESM-LR	0.0030	0.812
bcc-csm1-1-m	0.0033	0.792
EC-EARTH	0.0035	0.788
GFDL-ESM2G	0.0035	0.781
MIROC-ESM	0.0051	0.777
MPI-ESM-MR	0.0043	0.769
GFDL-ESM2M	0.0041	0.758
IPSL-CM5A-MR	0.0057	0.750
MIROC5	0.0075	0.734
CSIRO-Mk3-6-0	0.0058	0.731
CanESM2	0.0097	0.709
CESM1-CAM5	0.0106	0.690
HadGEM2-ES	0.0085	0.665
CCSM4	0.0164	0.618
HadGEM2-AO	0.0112	0.610
bcc-csm1-1	0.0154	0.553

drastic increase in atmospheric greenhouse gas concentration, spurred by increased anthropogenic carbon dioxide emissions, is represented by the RCP8.5 forcing scenario, in which elevated radiative forcing stabilizes at 8.5 W/m^2 by year 2100. Twenty-six models are available for the RCP2.6 scenario, and 39 models are available for the RCP8.5 scenario.

GCM monthly average rainfall depths were temporally downscaled to daily rainfall depths for the time period 1952–2050 using daily historical weather data from the airport weather stations on Yap (WMO Station 914130) and Pohnpei (WMO Station 913481). Gamma distributions for each month of the year were fitted to precipitation data for both the eastern and western FSM (see Fig. S-1 in Supplementary Data). Downscaled daily values then were statistically compared with historical daily values from 1952 to 2006 using the S_{score} and *BS* described in Section 2.2.2, with GCMs having an $S_{score} > 0.80$ accepted for use in RWCS design curve construction. Using the downscaled rainfall data for 2010–2050 for the accepted GCMs, the water balance algorithm of Eq. (1) is used with an efficiency ε of 70%. The daily household demand O_t is based on an average household size of four people each with a per capita water demand of 30 L/day, slightly above the United Nations minimum recommended provision of 20 L/day per capita to fulfill basic needs for drinking, cooking, and cleaning. Design curves representing 80%, 90%, and 95% reliability rates are constructed for the two RCP scenarios for each accepted GCM for both climate regions (western FSM and eastern FSM). An ensemble of design curves, with each curve representing a future possible climate scenario, therefore is constructed for each reliability level.

3. Results and discussion

3.1. Top-performing GCMs for the FSM

Assessment scores of the CMIP5 RCP2.6 scenario GCM model results for the eastern FSM region are presented in Table 2 in descending S_{score} value, with a line indicating the cut-off between the accepted ($S_{score} > 0.80$, Perkins et al., 2007) and rejected models for use in the RWCS design curve construction. Values of the *BS*, although not used in the direct acception/rejection of models, are used as a check of accepted models. S_{score} values ranged from 0.553 to 0.837, where models with a higher score show more overlap with the historical climate patterns, and *BS* values ranged from 0.002 to 0.015, where a smaller value indicates a better fit to historical data. As shown in Table 2, 11 of the 26 GCMs were accepted. CNRM-CM5 was the best performing model ($BS = 0.002$; $S_{score} = 0.837$), and bcc-csm1-1 was the worst performing model ($BS = 0.0154$; $S_{score} = 0.553$) for the eastern FSM.

Fig. 5a–c show a comparison between the PDF of the historical climate data and the PDF of the top three performing GCMs (CNRM-CM5, GISS-E2-R, and GFDL-CM3). For comparison, Fig. 5d shows a PDF comparison of the worst performing model (bcc-csm1-1). The significant overlap of the historical and simulated PDF is evident for the top three GCMs, whereas the lack of overlap is evident for the worst-performing GCM. Similar results are obtained for the RCP8.5 scenario for the eastern FSM region (see Table S-1 in Supplementary Data), with 16 of the 39 models accepted, with NorESM1-ME being the top-performing model

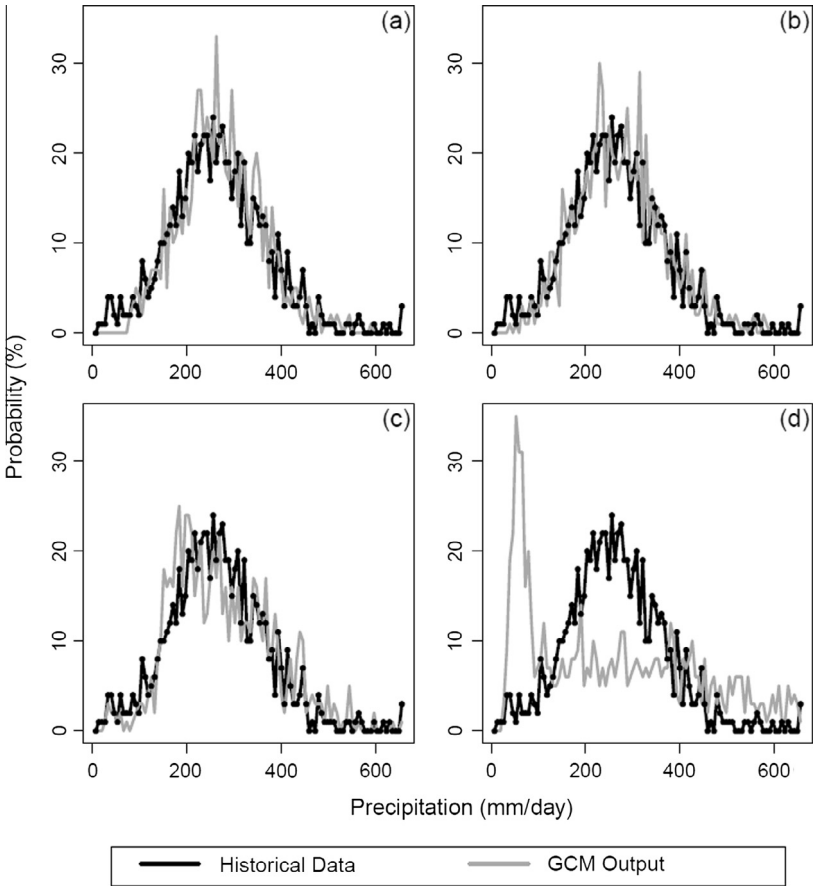

Fig. 5. Results of PDF comparison between GCM output and historical precipitation values for the eastern FSM region for the RCP2.6 forcing scenario. The three highest ranking GCMs are (a) CNRM-CM5, (b) GISS-E2-4, and (c) GFDL-CM3, with S_{score} values of 0.837, 0.834, and 0.833, respectively. The worst-performing GCM (d) is bcc-csm1-1, with an S_{score} of 0.553.

Please cite this article in press as: Wallace, C.D., et al. Rainwater catchment system design using simulated future climate data. J. Hydrol. (2015), http://dx.doi.org/10.1016/j.jhydrol.2015.08.006

(S_{score} = 0.868). Visual comparison between the PDFs of the historical and simulated rainfall depths for the top three performing models and for the worst-performing model is shown in Supplementary Data (Fig. S-1).

Tables of results for the western FSM are shown in Supplementary Data (Tables S-2 and S-3). In summary, 5 of the 26 models are accepted for the RCP2.6 scenario and 10 of the 39 models are accepted for the RCP8.5 scenario. Fig. 6 shows the comparison between the PDFs of the historical and simulated rainfall depths for the top three performing models and for the worst-performing model. The higher rainfall depths in eastern FSM can be seen in comparing Figs. 5 and 6, with the PDFs of eastern FSM

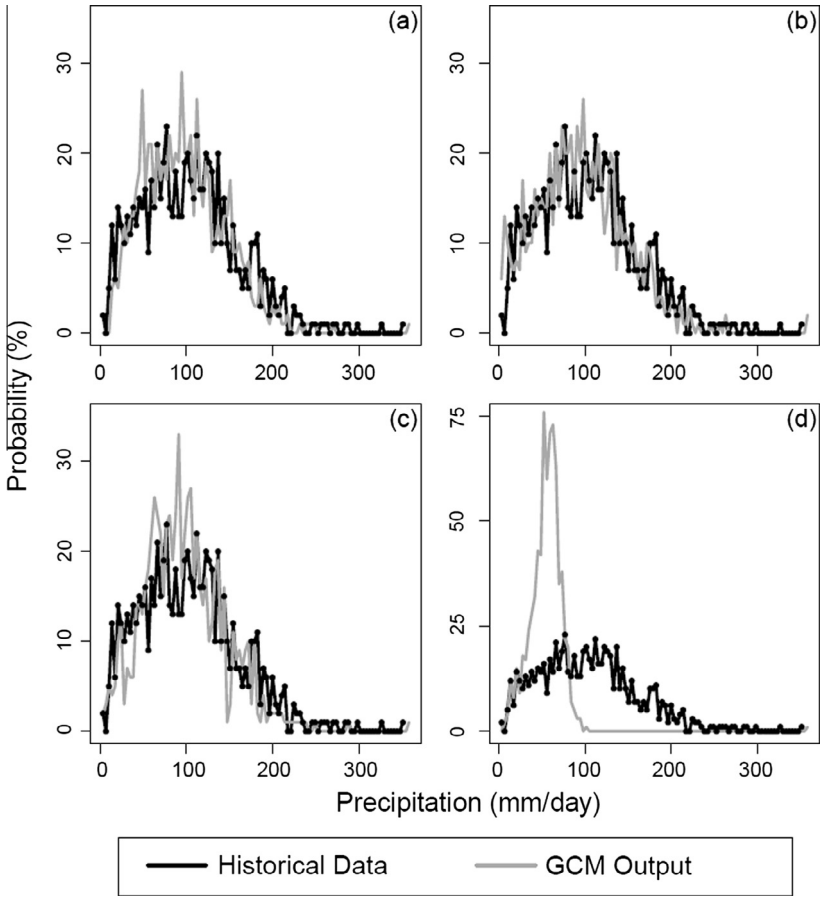

Fig. 6. Results of PDF comparison between GCM output and historical precipitation values for the western FSM region for the RCP2.6 forcing scenario. The best performing models in terms of the S_{score} are (a) GISS-E2-H, (b) GFDL-ESM2M, and (c) NorESM1-ME; the lowest performing is CSIRO-Mk3-6-0.

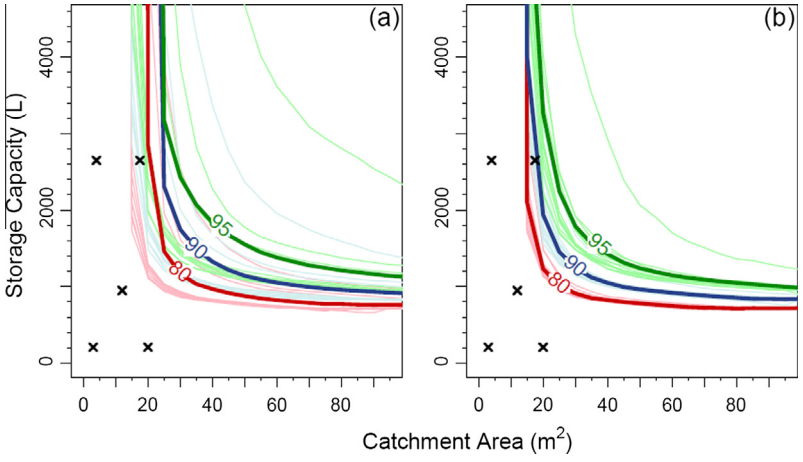

Fig. 7. RWCS design curves for the eastern FSM, developed for (a) the RCP2.6 and (b) RCP8.5 forcing scenarios, which size systems to supply no less than 120 L/day (demand of an average household of 4 people with an average water demand of 30 L/day per capita). Curves are shown for the 80%, 90%, and 95% reliability levels. The darker, thicker lines represent the curves developed using the average of the accepted GCM outputs, which are represented by the lighter lines. The capacity/catchment area combination of existing household RWCS in the community of Nikahlap Island are shown in (a) and (b).

Please cite this article in press as: Wallace, C.D., et al. Rainwater catchment system design using simulated future climate data. J. Hydrol. (2015), http://dx.doi.org/10.1016/j.jhydrol.2015.08.006

(Fig. 5) shifted to the right compared to the PDFs of western FSM (Fig. 6).

3.2. RWCS design curve construction

The RWCS design curves for the eastern and western FSM regions are shown in Figs. 7 and 8, respectively. For each level of reliability (80%, 90%, 95%), the design curve for each accepted GCM is shown, with the darker thick lines representing the design curve produced by averaging output from the accepted GCMs. Curves produced by averaged GCM output prevent extreme precipitation outliers from affecting the dataset, while also capturing the erratic nature of climate patterns for more conservative system design. No significant difference (<1%) was seen between curves developed using the averaged GCM values and the median of each dataset. For both figures, (a) shows results for the RCP2.6 scenario and (b) shows results for the RCP8.5 scenario. Although there is some overlap between the levels of reliability due to the spread of the individual GCM results, generally curves corresponding to lower reliability are shifted down and to the left of those with higher reliability; these findings are consistent with curves developed using historical precipitation data (Ngigi, 1999; Fewkes and Butler, 2000). Also, for each ensemble of curves (e.g. eastern FSM region, RCP2.6 shown in Fig. 7a) there is much more spread between the 95% reliability curves than for the 80% or 90% reliability curves, signifying differences between the GCMs in simulating the frequency and duration of low-rainfall periods. That is, some of the accepted GCMs have more periods of low rainfall, and hence

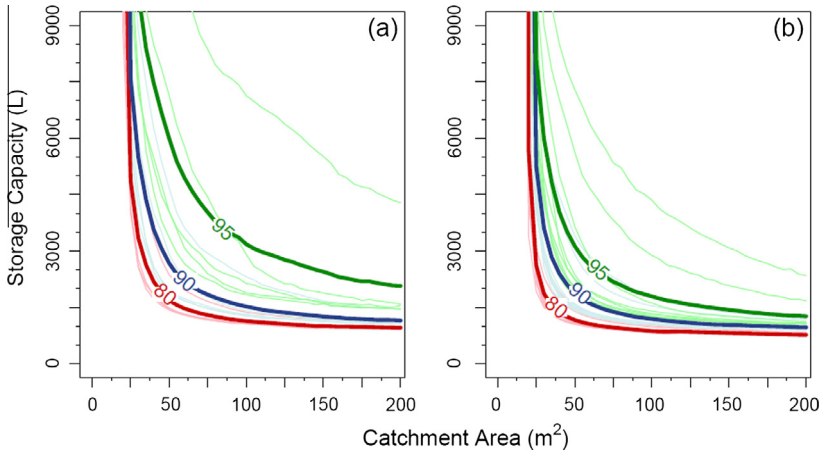

Fig. 8. RWCS design curves for the western FSM, developed for (a) the RCP2.6 and (b) RCP8.5 forcing scenarios, which size systems to supply no less than 120 L/day (demand of an average household of 4 people with an average water demand of 30 L/day per capita). Curves are shown for the 80%, 90%, and 95% reliability levels. The darker, thicker lines represent the curves developed using the average of the accepted GCM outputs, which are represented by the lighter lines.

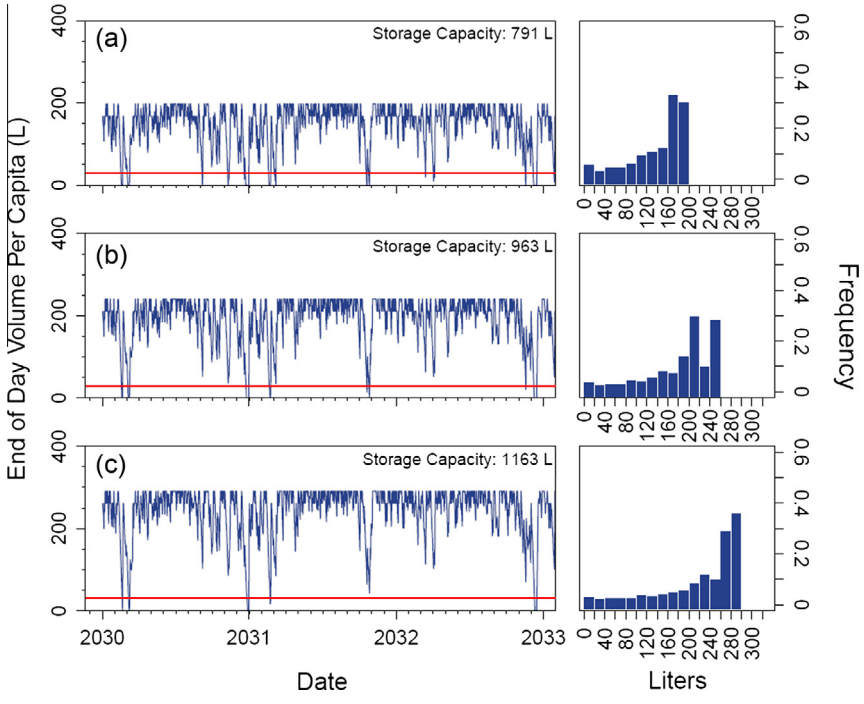

Fig. 9. (left) Time series of the end of day volume of stored rainwater per capita for the period 2030–2033 for (a) 80%, (b) 90%, and (c) 95% system reliability for the eastern FSM region. Selection of the study period was arbitrary, and intended to exemplify the trends seen in the volume of captured rainwater supply for the region. (right) Frequency distributions plots of stored rainfall volume.

Please cite this article in press as: Wallace, C.D., et al. Rainwater catchment system design using simulated future climate data. J. Hydrol. (2015), http://dx.doi.org/10.1016/j.jhydrol.2015.08.006

required a larger tank size for a given catchment area to achieve adequate stored rainwater volumes during these periods.

The system dimensions (storage capacity, rooftop catchment area) required to achieve a desired level of reliability are significantly higher for the western FSM region than for the eastern region. This is seen further in Figs. 9 and 10, which show example output from the water balance algorithm for the eastern and western FSM regions, respectively using results from one of the accepted GCMs. For the eastern FSM (Fig. 9), the time series for 2030–2033 is shown for three scenarios with a rooftop catchment area of 50 m^2: (a) uses a 791 L tank that results in 80% reliability, (b) uses a 963 L tank that results in 90% reliability, and (c) uses a 1163 L tank that results in 95% reliability, with the level of reliability indicated by the number of days that the end-of-day volume falls below the United Nations-recommended minimum requirement (indicated by red line). In contrast for the western FSM (Fig. 10), the three reliability levels require much larger tank sizes: 1070 L, 1457 L, and 1914, respectively, indicating the lower rainfall depths in the western FSM and hence the need for larger storage tanks. The level of reliability of each scenario also is demonstrated by the accompanying histograms of stored rainwater volume (to the right in Figs. 9 and 10), with more depletion occurring when smaller tanks are used. Relatively high levels of rainfall throughout Micronesia allow for smaller system dimensions when compared to systems in arid and semi-arid regions at the same rate of reliability (Ngigi, 1999; Basinger et al., 2010).

In some cases, nearly double the system dimensions (storage capacity, rooftop catchment area) are required for a RWCS to achieve 95% reliability than to achieve 80% reliability. For example, for the RCP2.6 scenario for the eastern region (Fig. 7a), using a catchment area of 40 m^2 requires a storage capacity of approximately 1000 L to achieve 80% reliability, whereas nearly 2000 L is required to achieve 95% reliability. For the western region (Fig. 8a), the required tank sizes are approximately triple (~1500 L for 80% reliability, ~4500 L for 95% reliability) for a catchment area of 75 m^2. For both regions, a catchment area of less than approximately 20 m^2 cannot achieve the desired reliability rates, indicated by the asymptotic increase of required storage capacity; conversely, a storage capacity of less than approximately 1000 L cannot achieve the desired reliability rates.

In general, the spacing and orientation of the design curves for the various reliability rates shifted not only regionally, but also amongst the RCP forcing scenarios. For the RCP8.5 scenario, which is characterized by increased emissions rates, the reliability curves are relatively clustered. In contrast, curves developed using output from the RCP2.6scenario, which represents extreme climate change mitigation via reduction of greenhouse gas emissions, are more dispersed. The difference in grouping infers more erratic rainfall patterns and decreasing annual rainfall depth for the RCP2.6 scenario as forecasted by the top-performing GCMs, ultimately making it more difficult for systems to achieve higher rates of reliability. Though the RCP2.6 forcing scenario is the lowest emission scenario, it shows a peak in atmospheric greenhouse gas concentration around year 2050 (van Vuuren et al., 2011), which could have a significant effect on climate patterns.

To meet water demand in the coming decades, the design curves presented in Figs. 7 and 8 can be used to size storage tanks and guttered roof areas for household RWCS in the FSM. To relate these design curves to example existing RWCS designs in the FSM, the dimensions of the eight household RWCS serving the Nikahlap community located on Pakein Atoll, Pohnpei State (eastern FSM) are shown in Fig. 7a and b. Three of the systems have higher storage capacities (5700 L, 5700 L, 7190 L) than are shown in Fig. 7, with associated roof catchment areas of 16 m^2, 20 m^2, and 10 m^2 (Wallace and Bailey, 2014). Of the 8 systems, 6 (four shown, and the 5700 L/16 m^2 and 7190 L/10 m^2 systems) currently are not adequate to meet future demand. Thus, each of these systems should be resized to perform at the community's desired reliability rate; in some cases both the catchment area and storage capacity require expansion. When using the presented design curves for RWCS dimension sizing, the average value (thick, dark curve in the figures) could be used, although a more conservative (yet more costly) approach is to use the GCM curve that requires the largest dimensions. For the 95% reliability however, this latter approach

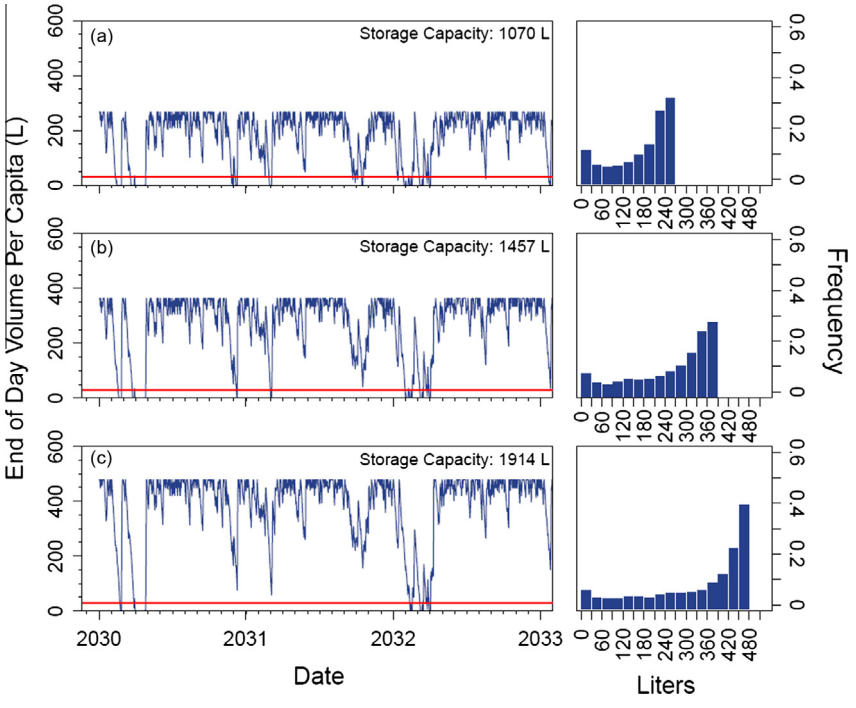

Fig. 10. (left) Time series of the end of day volume of stored rainwater per capita for the period 2030–2033 for (a) 80%, (b) 90%, and (c) 95% system reliability for the western FSM region. Selection of the study period was arbitrary, and intended to exemplify the trends seen in the volume of captured rainwater supply for the region. (right) Frequency distributions plots of stored rainfall volume.

Please cite this article in press as: Wallace, C.D., et al. Rainwater catchment system design using simulated future climate data. J. Hydrol. (2015), http://dx.doi.org/10.1016/j.jhydrol.2015.08.006

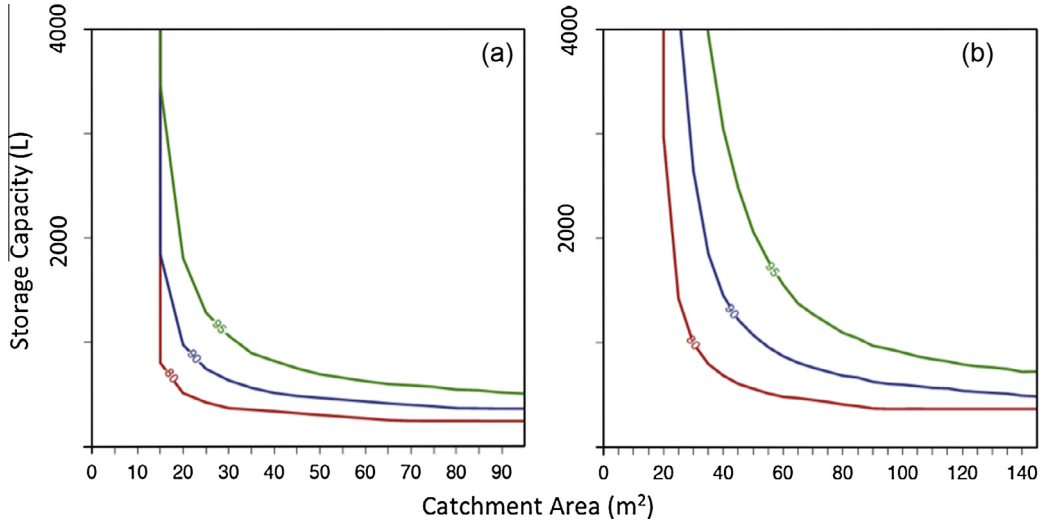

Fig. 11. RWCS design curves developed for the eastern (a) and western (b) FSM using historical precipitation data from 1952 to 2012. Though the curves show a similar distribution to those developed using simulated future climate data, system size is drastically reduced.

likely is not practical, and hence other water supply sources should be found in case of prolonged periods of drought. This is particularly crucial for the atoll island communities, which cannot rely on surface water storage for supplementing RWCS supply.

To investigate the potential effects of climate change on the sustainable design of RWCS, design curves were also developed using historical daily precipitation data from 1952 to 2012 (Fig. 11). Though the curves for both regions show similar shape and distribution to those developed using simulated future climate data, the recommended system sizes are reduced, particularly for the eastern FSM. For example, at 80% reliability the curves developed for the eastern FSM (Fig. 7) show that approximately 1000 L of storage capacity is required for 40 m^2 of catchment area, while the curves developed using the historical data indicate that a storage capacity of only about 500 L is required (Fig. 11a). The strong variation in required system size between historical and future climate data highlights the need for RWCS design based on projected changes in climate patterns, as is performed in this study.

4. Summary and conclusions

This paper presents a new methodology to develop rainwater catchment systems (RWCS) design curves using projected rainfall patterns from General Circulation Models (GCMs). The design curves comprise the ensemble of storage tank size (L) and roof catchment areas (m^2) combinations that yield a given level of reliability (80%, 90%, 95%) based on projected future rainfall depth magnitudes and temporal patterns. Curves developed allow for reliable design without the need for system modeling, providing communities with an easily applied method for sizing household systems based on demand. Consistently reliable RWCS performance can help ensure adequate water supply, especially in water-scarce regions where groundwater sources are either excessively contaminated or unavailable. The method is applied to the eastern and western regions of the Federated States of Micronesia (FSM), a nation of islands in the western Pacific for which captured rainwater by RWCS is a major source of water supply.

The design curves presented in this paper are intended to assist communities in sizing household-scale RWCS with reliability rates sufficiently high to provide adequate water supply, especially during periods of low rainfall. The reliability rates considered in this study (80%, 90%, 95%) were selected due to the high level of dependence of FSM island communities on RWCS to supply potable water. For atoll islands, which typically are isolated geographically from neighboring islands and have no surface water reserves, the 95% reliability rate curve is recommended for RWCS design. For the four high volcanic islands (Yap, Chuuk, Pohnpei, Kosrae), for which surface water resources can be used to supplement RWCS stored volumes, the 80% and 90% reliability rate curves are recommended. To achieve the desired rates of reliability, systems designed for the western FSM require dimensions much larger than those for the eastern FSM due to lower rainfall rates in the western region. Furthermore, comparison with design curves constructed using historical precipitation data indicates that constructing RWCS using historical data will result in under-sizing the system.

The method described in this paper can be applied generally to geographic regions worldwide, with any level of reliability desired based on the needs of the region, e.g. to use RWCS to supplement surface water and groundwater, to manage urban stormwater flow volumes, or to facilitate green building applications.

Appendix A. Supplementary material

Supplementary data associated with this article can be found, in the online version, at http://dx.doi.org/10.1016/j.jhydrol.2015.08.006.

References

Abdulla, F.A., Al-Shareef, A.W., 2009. Roof rainwater harvesting systems for household water supply in Jordan. Desalination, 195–207.
Bailey, R.T., Jenson, J.W., Taborosi, D., 2013. Estimating the freshwater lens thickness of atoll islands in the Federated States of Micronesia. Hydrogeol. J., 441–457.
Basinger, M., Montalto, F., Lall, U., 2010. A rainwater harvesting system reliability model based on nonparametric stochastic rainfall generator. J. Hydrol. 392, 105–118.
Bates, B.C., Charles, S.P., Hughes, J.P., 1998. Stochastic downscaling of numerical climate model simulations. Environ. Modell. Softw., 325–331.
Biazin, B., Sterk, G., Temesgen, M., Abdulkedir, A., Stroosnijder, L., 2012. Rainwater harvesting and management in rainfed agricultural systems in Sub-Saharan Africa – a review. Phys. Chem. Earth, 139–151.
Brier, G.W., 1950. Verification of forecasts expressed in terms of probability. Mon. Weather Rev., 1–3.
Charles, S.P., Bates, B.C., 1999. A spatiotemporal model for downscaling precipitation occurence and amounts. J. Geophys. Res., 31657–31669.

Chilton, J., Maidment, G., Marriott, D., Francis, A., Tobias, G., 1999. Case study of a rainwater recovery system in a commercial building with a large roof. Urban Water, 345–354.
CIRIA, 2001. Rainwater and Greywater Use in Buildings: Best Practice Guidance. CIRIA Publication C539.
Coe, R., Stern, R., 1982. Fitting models to daily rainfall data. J. Appl. Meteorol., 1024–1031.
Coombes, P., Argue, J., Kuczera, G., 1999. Figtree Place: a case study in water sensitive urban development (WSUD). Urban Water 1, 335–343.
Cowden, J., Watkins, J.D., Mihelcic, J., 2008. Stochastic rainfall modeling in West Africa: parsimonious approaches for domestic rainwater harvesting assessment. J. Hydrol. 361, 64–77.
Diagger, 2009. Evolving urban water and residuals management paradigms: water reclamation and reuse, decentralization, and resource recovery. Water Environ. Res., 809–822.
Dillaha, T.A., Zolan, W.J., 1985. Rainwater catchment water quality in Micronesia. Water Resour., 741–746.
Dixon, A., Butler, D., Fewkes, A., 1999. Water saving potential of domestic water reuse systems using greywater and rainwater in combination. Water Sci. Technol. 29 (5), 25–32.
Fewkes, A., 1999. The use of rainwater for WC flushing: the field testing of a collection system. Build. Environ., 765–772.
Fewkes, A., Butler, D., 2000. Simulating the performance of rainwater collection and reuse systems using behavioural models. Build. Serv. Eng. Res. Technol., 99–106.
Fu, G., Liu, Z., Charles, S.P., Xu, Z., Yao, Z., 2013. A score-based method for assessing the performance of GCMs: a case study of southeastern Australia. J. Geophys. Res.: Atmos., 4154–4167.
Ghisi, E., 2006. Potential for potable water savings by using rainwater in the residential sector of Brazil. Build. Environ. 41, 1544–1550.
Ghisi, E., Bressan, D., Martini, M., 2007. Rainwater tank capacity and potential for potable water savings by using rainwater in the residential sector of southeastern Brazil. Build. Environ., 1654–1666.
Gould, J., Nissen-Petersen, E., 1999. Rainwater Catchment Systems for Domestic Supply. In: Practical Action.
Guo, Y., Baetz, B.W., 2007. Sizing of rainwater storage units for green building applications. J. Hydrol. Eng., 197–205.
Han, M., Ki, J., 2010. Establishment of sustainable water supply systems in small islands through rainwater harvesting (RWH): case study of Guja-do. Water Sci. Technol. (WST), 148–153.
Helmreich, B., Horn, H., 2008. Opportunities in rainwater harvesting. Desalination.
Herrmann, T., Schmida, U., 1999. Rainwater utilisation in Germany: efficiency, dimensioning, hydraulic and environmental aspects. Urban Water 1, 307–316.
Jenkins, D., Pearson, F., Moore, E., Sun, J.K., Valentine, R., 1978. Feasibility of Rainwater Collection Systems in California. California Water Resources Center, Contribution No. 173.
Jones, M.P., Hunt, W.F., 2010. Performance of rainwater harvesting systems in the southeastern United States. Resour., Conserv. Recycl., 623–629.
Khastagir, A., Jayasuriya, N., 2010. Optimal sizing of rain water tanks for domestic water conservation. J. Hydrol. 381, 181–188.
Lall, U., Rajagopalan, B., Tarboton, D., 1996. A nonparametric wet/dry spell model for resampling daily precipitation. Water Resour. Res. 32 (9), 2803–2823.
Lander, M.A., Khosrowpanah, S., 2004. Rainfall Climatology for Pohnpei Islands, Federated States of Micronesia. Water and Environmental Research Institute of the Western Pacific (WERI), Technical Report No. 103.
Lanzante, J., 1996. Resistant, robust and non-parametric techniques for the analysis of climate data: theory and examples, including applications to historical radiosonde station data. Int. J. Climatol. 16, 1197–1226.
Li, Z., Boyle, F., Reynolds, A., 2010. Rainwater harvesting and greywater treatment systems for domestic application in Ireland. Desalination, 1–8.
Liaw, C.H., Tsai, Y.L., 2004. Optimum storage volume of rooftop rain water harvesting systems for domestic use. J. Am. Water Resour. Assoc., 901–912.
Liaw, C.-H., Chiang, Y.-C., 2014. Dimensionless analysis for designing domestic rainwater harvesting systems at the regional level in Northern Taiwan. J. Water, 3913–3933.
MacCracken, R.S., Jenson, J.W., Heitz, L.F., Rubinstein, D.H., Mylroie, J.E., 2007. Water Resources Analysis of Fais Island, Federated States of Micronesia. Water and Environmental Research Institute of the Western Pacific (WERI), Technical Report No. 111.
Mearns, L.O., Giiorgi, F., McDaniel, L., Shields, C., 1995. Analysis of daily variability of precipitation in a nested regional climate model: comparison with observations and doubled CO_2 results. Glob. Planet. Change, 55–78.
Meehl, G., Goddard, L., Murphy, J., Stouffer, R.J., Boer, G., Danabasoglu, G., et al., 2009. Decadal prediction: can it be skillful? Am. Meteorol. Soc., 1467–1485.
Micronesia, F.S., 2002. FSM Census of Population and Housing. Government of the Federated States of Micronesia, Division of Statistics, Palikir, Pohnpei.
Mitchell, V., 2007. How important is the selection of computational analysis method to the accuracy of rainwater tank behaviour modelling? Hydrol. Process., 2850–2861.
Mun, J., Han, M., 2012. Design and operational parameters of a rooftop rainwater harvesting system: definition, sensitivity, and verification. J. Environ. Manage., 147–153.
Ngigi, S.N., 1999. Optimization of rainwater catchment systems design parameters in the arid and semiarid lands of Kenya. In: Ninth International Rainwater Conference.
Opare, S., 2012. Rainwater harvesting: an option for sustainable rural water supply in Ghana. GeoJournal, 695–705.
Oweis, T., Hachum, A., 2006. Water harvesting and supplemental irrigation for improved water productivity of dry farming systems in West Asia and North Africa. Agric. Water Manage. 80, 57–73.
Palla, A., Sansalone, J.J., Gnecco, I., Lanza, L.G., 2011. Storm water infiltration in a monitored green roof for hydrologic water restoration. Water Sci. Technol., 766.
Perkins, S.E., Pitman, A.J., Holbrook, N.J., McAneney, J., 2007. Evaluation of the AR4 climate models' simulated daily maximum temperature, minimum temperature, and precipitation over Australia using probability density functions. J. Climate, 4356–4376.
Roebuck, R.M., Ashley, R.M., 2006. Predicting the hydraulic and life-cycle cost performance of rainwater harvesting systems using a computer based modelling tool. In: Seventh International Conference on Urban Drainage and Fourth International Conference on Water Sensitive Urban Design, Melbourne, pp. 2699–2706.
Rowe, M.P., 2011. Rain water harvesting in Bermuda. J. Am. Water Resour. Assoc., 1219–1227.
Sharma, A., Lall, U., 1999. A nonparametric approach for daily rainfall simulation. Math. Comput. Simulat., 261–371.
Srikanthan, R., 2005. Stochastic generation of daily rainfall data. CRC Catchment Hydrol., 1915–1921.
Srikanthan, R., McMahon, T.A., 2001. Stochastic generation of annual, monthly and daily climate data: a review. Hydrol. Earth Syst. Sci., 653–670.
Steffen, J., Jensen, M., Pomeroy, C., Burian, S., 2013. Water supply and stormwater management benefits of residential rainwater harvesting in U.S. cities. J. Am. Water Resour. Assoc. 49 (4), 810–824.
Sturm, M., Zimmermann, M., Schutz, K., Urban, W., Hartung, H., 2009. Rainwater harvesting as an alternative water source in rural sites in central northern Namibia. Phys. Chem. Earth, 776–785.
Su, M.-D., Lin, C.-H., Chang, L.-F., Kang, J.-L., Lin, M.-C., 2009. A probabilistic approach to rainwater harvesting systems design and evaluation. Resour., Conserv., Recycl. 53, 393–399.
Taboroši, D., Collazo, M.S., 2011. Mwoakilloa Atoll: freshwater resources and their usage, state, and infrastructure. Island Res. Educ. Initiative.
Taboroši, D., Martin, M., 2011. Pakein Atoll: freshwater resources and their usage, state, and infrastructure. Island Res. Educ. Initiative.
Taylor, K.E., Stouffer, R.J., Meehl, G.A., 2012. An Overview of CMIP5 and the experiment design. Bull. Am. Meteorol. Soc. 93, 485–498.
Todorovic, P., Woolhiser, D.A., 1975. A Stochastic model of n-day precipitation. J. Appl. Meteorol., 17–24.
van Vuuren, D., Edmonds, J., Kainuma, M., Riahi, K., Thomson, A., Hibbard, K., et al., 2011. The representative concentration pathways: an overview. Climatic Change 109, 5–31.
Wallace, C.D., Bailey, R.T., 2014. Sustainable rainwater catchment systems for Micronesian Atoll Communities. J. Am. Water Resour. Assoc. (JAWRA), 1–15.
Walsh, K.J., McGregor, J.L., 1997. An assessment of simulations of climate variability over Australia with a limited area model. Int. J. Climatol., 201–223.
Walsh, K.J., McGregor, J.L., 1995. January and July climate simulations over the Australian region using a limited-area model. Climate, 2387–2403.
Ward, S., Memon, F.A., Butler, D., 2010. Rainwater harvesting: model-based design evaluation. Water Sci. Technol., 85–96.
White, I., Falkland, T., Perez, P., Dray, A., Metutera, T., Metai, E., et al., 2007. Challenges in freshwater management in low coral atolls. J. Clean. Prod., 1522–1528.
Zhang, D., Gersberg, R., Wilhelm, C., Voigt, M., 2009. Decentralized water management: rainwater harvesting and greywater reuse in an urban area of Beijing, China. Urban Water J. 6 (5), 375–385.

Please cite this article in press as: Wallace, C.D., et al. Rainwater catchment system design using simulated future climate data. J. Hydrol. (2015), http://dx.doi.org/10.1016/j.jhydrol.2015.08.006